Final Report
National Oceanic and Atmospheric Administration (NOAA)
Joint Hurricane Testbed (JHT) Program

Improved SFMR Surface Wind Measurements in Intense Rain Conditions

Principal Investigator: Eric W. Uhlhorn, NOAA/AOML/Hurricane Research Division
Co-investigator: Bradley W. Klotz, University of Miami/CIMAS/Hurricane Research Division

Abstract:

The airborne stepped frequency microwave radiometer (SFMR) estimates surface winds and rain rate in most weather conditions, particularly in tropical cyclones. However, retrieval accuracy has been shown to be biased high in weak-to-moderate winds coupled with strong precipitation. The objective of this two-year project was to quantify the wind speed errors in such situations and propose a solution that may be implemented for real-time operations. In the first year, the primary goal was to provide an empirically-determined SFMR wind speed bias correction computed from the wind speed and rain rate reported in the HDOB messages. For year two of this project, the main objectives were to evaluate the performance of the wind speed bias correction and to develop an updated geophysical model function that reduces the rain contamination problem. The following report provides an overview of the key results throughout the work as well as the remaining updates from the second half of year-2. Final updated results from the remainder of year-2 indicate that a major source of the high bias in the SFMR wind speeds derives from incorrect rain absorption estimation. An improved relationship between rain and absorption is developed using independent precipitation data, and a more accurate relationship between wind speed and surface emissivity is developed to provide a more representative geophysical model function. A statistical analysis of the updated function compared to the current operational version is provided to demonstrate the improvements.

Key results and accomplishments from year-1 to mid-year-2:

Before we describe the additional updates and accomplishments achieved during the second half of year-2, it is useful to provide an overview of the key results that were previously obtained. As one of our main motivating points for conducting this work, it was stipulated that the SFMR wind speeds were biased high in the presence of heavy precipitation. In order to verify this bias, the authors reported the

necessary collection of coincident dropsonde and SFMR winds. Initially, we collected data between 2005 and 2011, but we were able to incorporate coincident data from 1999 up through 2012 by the mid-point of year-2. While there were numerous dropsondes available within this time period, it was determined that there were too few data in the presence of moderate to heavy rain. Therefore, a synthetic wind speed was developed from a relationship between flight-level winds and the WL150 dropsonde reported wind speed (see preliminary project reports for methodology and details). These winds were used to supplement precipitation regions of the database that were lacking a robust sample size. The flight patterns of many of the research and reconnaissance flights are not specifically designed to target precipitating regions with dropsondes, which is why initially few observations were available. During the 2012 Atlantic hurricane season, intentional efforts were conducted to collect dropsonde winds in precipitation, but there were still several gaps containing sufficient samples. Table 1 below provides the most up-to-date database for the coincident SFMR wind speed and dropsonde surface-adjusted wind speed pairs.

	$0 \le U_{SFMR} < 17$	$17 \le U_{SFMR} < 25$	$25 \le U_{SFMR} < 33$	$33 \le U_{SFMR} < 50$	$U_{SFMR} \ge 50$
$0 \le R < 10$	1356 (0)	690 (0)	354 (0)	196 (0)	27 (0)
$10 \le R < 20$	16 (38)	73 (219)	124 (166)	134 (101)	21 (4)
$20 \le R < 30$	5 (18)	12 (84)	44 (48)	69 (75)	24 (12
$R \ge 30$	1 (4)	7 (12)	18 (11)	48 (41)	23 (34)

Table 1. SFMR wind speed and GPS dropsonde surface-adjusted wind speed pairs for 1999-2012. Columns are SFMR wind speed bins and rows are SFMR rain rate bins. Values in parentheses are synthetic wind speeds for a particular bin. Wind speed values are in m s^{-1} and rain rates are in mm hr^{-1}.

Based on the pairs provided in Table 1, a wind speed bias correction model was developed. A working version was used by the National Hurricane Center (NHC) during the 2012 season, but an update was provided for the 2013 season (see Figure 1). This correction model indicates that the largest bias is typically found for weak wind speeds and heavy precipitation but also a small high bias exists at weak winds without the influence of precipitation. The bias correction function is:

$$\delta U = -6.79 \cdot 10^{-2} U_{SFMR} + 9.36 \cdot 10^{-2} R - 3.90 \cdot 10^{-4} U_{SFMR} R + 3.06 \quad (\mathrm{m\,s^{-1}}) \qquad (1)$$

where δU is the bias, U_{SFMR} is the SFMR wind speed and R is the SFMR rain rate.

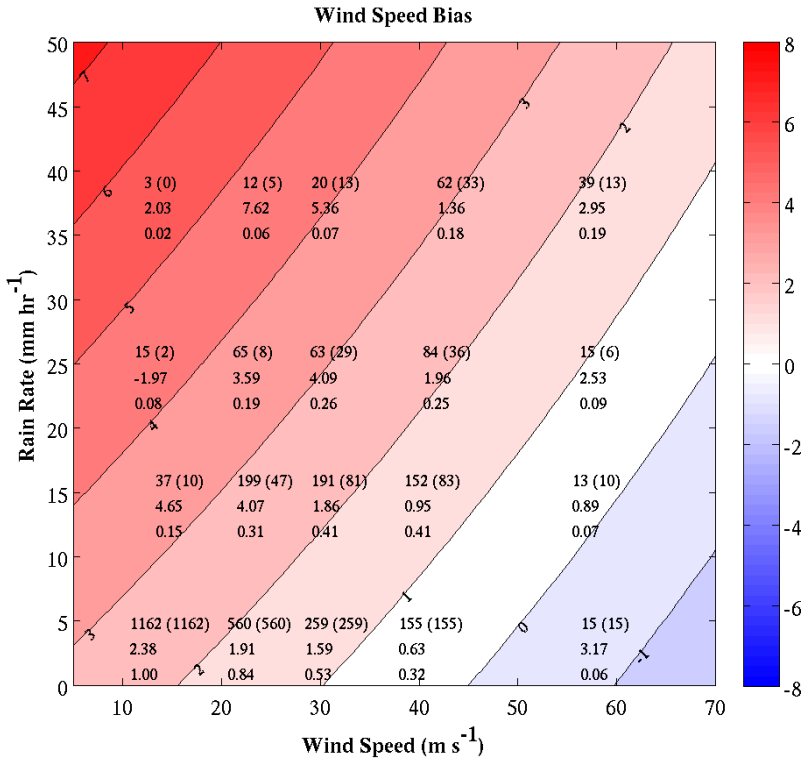

Figure 1. The overall SFMR wind speed bias correction model based on an 80% random sample is graphically shown. Large positive biases correspond with red colors, and large negative biases correspond with blue colors. Text on the figure are based on the wind speed and rain rate bins and indicate the total number of pairs (with real pairs in parentheses), the bin-mean wind speed bias, and the bin standard deviation weight applied during the model development.

The bias correction was applied to an independent sample of wind speed pairs and it was determined that for the overall wind speed population, the bias was reduced to less than 1 m s^{-1}. For conditions of weak wind and heavy precipitation, the bias and root mean squared error both were reduced by more than 50%. The bias correction model was determined to be valid for operational use (in-house) at NHC. Therefore, the key results up to the early to middle portion of year-2 are that the wind speed pair database was completed, that the bias correction model was developed and performed as expected, that the bias correction model successfully reduced the bias in most situations and was successfully utilized in real-time by hurricane specialists for their forecasts. This wind speed bias correction was successfully transferred to the necessary representatives at NHC for their use.

Updates from the remainder of year-2:

For the remainder of the JHT performance period, the following goals still remained to be

addressed:

1) *March – April 2013:* Coordinate installation of statistical correction on the NOAA and Air Force Reserve aircraft
2) *May 2013:* Complete development of updated, coupled GMF
3) *June – August 2013:* Test and evaluate SFMR winds computed from updated GMF for all AFRC and NOAA missions
4) *August 2013:* Provide software and documentation to NOAA/AOC, 53rd WRS, and ProSensing, Inc. for possible real-time implementation

Task 1:

It was understood that the statistical bias correction would not need to be installed on aircraft because the winds were being corrected at NHC. Also, the update to the GMF would render the need for this correction on the aircraft to be unnecessary.

Task 2:

In order to complete the update to the GMF, the wind versus emissivity relationship was evaluated. The current operational version was based on a dataset that contained only 160 pairs (Uhlhorn et al., 2007), very few of which were within precipitation or heavy precipitation. In order to improve the relationship, a larger sample of data were used (1513 paired samples) and for wind speeds less than 35 m s^{-1}, pairs were rejected if $R > 2$ mm hr^{-1} in order to remove any impact from rain on the emissivity within weaker wind regimes. Also, emissivity values for comparison were only taken from the lowest SFMR frequency (4.74 GHz) because this channel is expected to be the least affected by rain and is therefore the best option for obtaining a rain free relationship between wind and emissivity. The emissivity using the 4.74 GHz channel is compared with the surface-adjusted wind speed from the dropsondes and the updated relationship is provided in Figure 2 along with the current operational version.

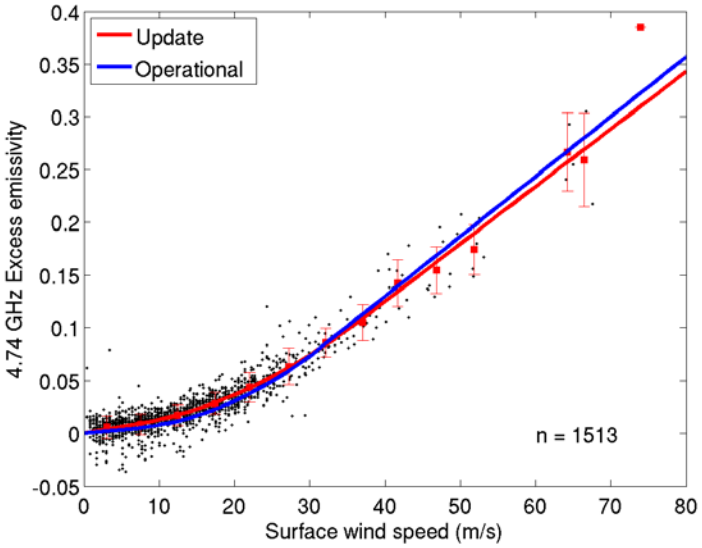

Figure 2. Emissivity at 4.74 GHz plotted as a function of the surface-adjusted dropwindsonde wind speed. The black dots are individual samples and the red (blue) lines indicate the function for the updated (operational) versions. The red squares are bin-averaged samples with 95% confidence intervals (error bars) for the proposed update.

Generally, the current operational version, which was developed from the limited data sample, appears remarkably accurate as compared to the updated function determined here based on the much larger sample size. The root mean squared error of the fit is 0.012 (or, ~3.5 K at *SST* = 28 °C, which is nearly equal to the emissivity error in the operational version). The most significant difference is found in the 10-20 m s^{-1} range, where emissivity values are higher, although the difference is quite small, being within the excess emissivity noise level. The fact that these two model functions are very similar in magnitude indicates that the emissivity may not directly be the cause of the high SFMR wind speed bias. A functional form identical to the operational model consisting of two linear functions connected at intermediate wind speeds with a quadratic function is fit (Eq. (2) below) to the observations with a constrained piecewise regression algorithm. As before, the low-wind breakpoint (w_l) is set to 7 m s^{-1}, where wave breaking and foam begins to occur (e.g., Monahan, 1971; Ross and Cardone, 1974), and the high-wind breakpoint (w_u) is determined via trial-and-error to minimize the root mean squared error of the fit, which here is found to be 37.0 m s^{-1}:

$$\varepsilon_w(4.74\ \text{GHz}) = \begin{cases} 1.232\times10^{-3}U_{sfc} & (0 \le U_{sfc} < 7.0) \\ 2.02\times10^{-3} + 1.515\times10^{-4}U_{sfc} + 4.122\times10^{-5}U_{sfc}^2 & (7.0 \le U_{sfc} < 37.0) \\ -6.294\times10^{-2} + 3.424\times10^{-3}U_{sfc} & (U_{sfc} \ge 37.0) \end{cases}$$

(2)

Historically, the small excess emissivity dependence on frequency in the operational model function was based on passive microwave observations of the sea surface (Webster et al., 1976), but until now was not verified for SFMR applications. The operational excess emissivity sensitivity to frequency is given as $\varepsilon'_w = 0.15\varepsilon_w$. We computed the slope of ε_w vs. wind speed for the large sample of SFMR vs. dropsonde surface wind speed shown in Fig. 2. Considering observational uncertainties, the computed results compare quite well with the operational version, indicating previous results should remain acceptable. We choose to implement a revised slope function as part of the model function update, according to:

$$\varepsilon'_w = a_0 + a_1 U_{sfc} + a_2 U_{sfc}{}^2, \quad (3)$$

where the coefficients determined from a least-squares regression are 2.7875×10^{-4}, 1.8602×10^{-5}, and 5.1662×10^{-6}. The proposed complete emissivity-wind (ε_w – W) geophysical model function now reads:

$$\varepsilon_w(f) = \varepsilon_w(4.74, U_{sfc}) + \varepsilon'_w(U_{sfc})\Delta f\ , \quad (4)$$

where Δf is the SFMR channel frequency minus 4.74 GHz.

With the wind portion of the GMF updated, the rain-absorption portion of the algorithm needs to be addressed. For our purposes, the impact of precipitation on SFMR brightness temperature is estimated by computing a microwave absorption coefficient, nominally a function of liquid water content and frequency. The operationally implemented model function (Uhlhorn and Black 2003) was incrementally developed based on radar reflectivity observations in hurricanes. SFMR rain rate retrievals were examined based other sources of precipitation observations (Jiang et al. 2006), and results of an inter-comparison with radar-derived rain rates indicated a tendency for overestimating weak rain rates and underestimating strong rain rates. It was concluded a possible cause for this anomalous behavior was uncertainty in estimating the height of the rain column. In the operational implementation, the height of the rain column (i.e., the freezing level) is set to a constant 4 km depth above the surface. In the calculations of absorption coefficient for this work, the freezing level (H) is estimated from the aircraft flight-level temperature and altitude according to a typical hurricane temperature profile:

$$H = a + T_a \gamma^{-1}, \quad (5)$$

where a is the aircraft radar altitude (m), T_a is the ambient temperature (C), and $\gamma = 5.22\times10^{-3}$ C m^{-1} is the lapse rate determined from a large database assembled by Zhang and Uhlhorn (2012) of dropsonde

temperature profiles obtained in hurricanes.

The current operational absorption vs. rain rate (κ-R) relationship is based primarily on radar reflectivity-derived rain rates computed by Jorgensen and Willis (1982) in hurricane conditions. The JW82 reflectivity vs. rain rate (Z-R) relationship is $Z = 300R^{1.35}$, where R is in mm hr^{-1} and Z in mm^6 m^{-3}. With more data resources available, along with significant improvements to instrumentation, we revisited this relationship in light of the SFMR rain rate retrievals. Specifically path-averaged TDR reflectivity data are compared with in situ Droplet Measurement Technologies Precipitation Imaging Probe (PIP) rain rate data obtained in several recent aircraft missions in tropical cyclones.

Layer-mean TDR reflectivity values are vertically averaged from just above the sea surface (to eliminate sea clutter) to the freezing level and are computed for 11 radial legs in two hurricanes [six in Hurricane Katrina (2005) and five in Hurricane Earl (2010)]. The bright band, which can increase the reflectivity up to 7 dB in the reflectivity below the 0 °C isotherm due to melting precipitation (Rinehart 2004), is filtered out. These flights were chosen due to reasonable high quality of PIP data. For the 11 flights, a sample of 1,836 collocated TDR dBZ and PIP dBR data is obtained. Samples for reflectivity <3 dBZ or when PIP sampling volume is <200 l^{-1} are rejected, since ultimately the SFMR is unable to measure such weak precipitation. Cumulative distributions of TDR and PIP observations are shown in Fig 3b.

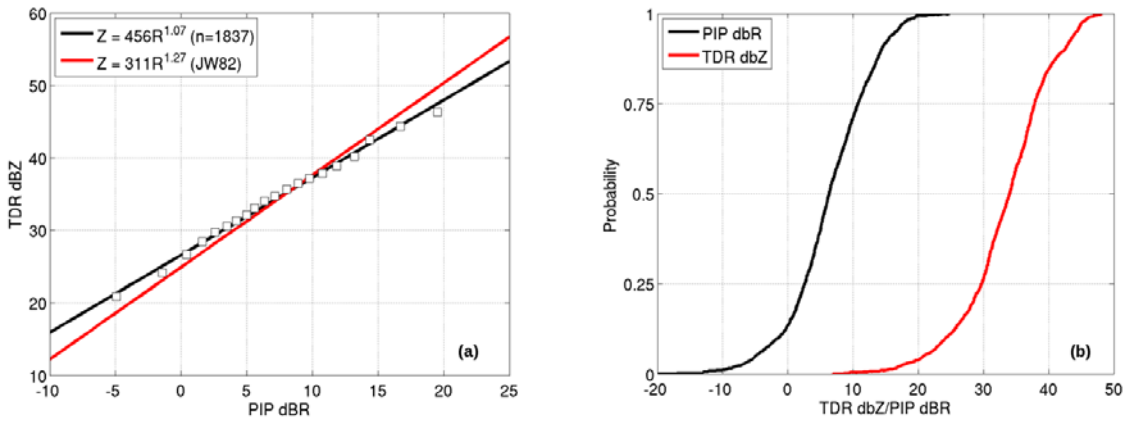

Figure 3. In (a), the rain values from the PIP are related to the TDR reflectivity (black) in a logarithmic reference frame based on probability matching. The markers indicate the matched PIP and TA rain products from 1% to 99%. The regression fit for this data is provided along with the original relationship from Jorgensen and Willis (1982) in red. Cumulative distribution functions for the PIP rain rate (black, dBR) and TA column-mean reflectivity (red, dBZ) are shown in (b) and are used to provide the range of expected rain rates.

As depicted in Fig. 3, median reflectivity and rain rate are ~33 dbZ and ~6 dbR (~3 mm hr^{-1}),

respectively. Variances for each quantity are reasonably comparable, although the PIP has a larger weak precipitation tail. Maximum reflectivity in this sample is ~49 dbZ. Peak rain rates are ~25 dbR (~316 mm hr^{-1}), although such extreme values are highly infrequent, and would likely not be detected by the SFMR due to its far larger sampling volume.

Additionally, a new *Z-R* relationship is computed using probability matching (e.g., Rosenfeld et al., 1993; Rosenfeld et al., 1994), in which observations at specified percentile levels for each data are correlated. Probability levels from 1 to 99% are shown on a log scale in Fig. 3a. A linear fit to these data results in the following Z-R relationship: $Z = 456R^{1.07}$. For the median rain rate, each function yields very similar reflectivity values, but the results here suggest a weaker radar sensitivity to rain rate than indicated by the JW82 results (i.e., a smaller rain rate exponent). Some of this sensitivity loss could be due to the vertical averaging and inherent smoothing of the reflectivity data, and therefore represents a far larger spatial scale than the in situ rain rates. However, the layer mean value is more representative of the path-averaged microwave brightness temperatures observed by SFMR, to which radar-derived rain rates are correlated.

SFMR observations and TDR reflectivity vertical profiles are obtained from 26 radial legs in three hurricanes [14 in Rita (2005), 5 in Felix (2007), 7 in Bill (2009)]. The surface emissivity is computed from the "corrected" SFMR retrieved wind speed using Eq. (3). Layer-averaged radar-derived rain rate at the SFMR observation location is calculated from the *Z-R* relationship found in this study. Over 21000 samples of κ at each channel are paired with the collocated rain rate. The cumulative probability distributions of κ and R are matched from the 1% to 99% levels (Fig. 4), and linear fits to the data (in log space) are made. Below ~5 dbR (3 mm hr^{-1}) which corresponds to ~30 dbZ, the signal appears to be lost, indicating the lower limit of SFMR sensitivity. The highest 1% of rain rates is >55 mm hr^{-1}, whereas operationally-measured rain rates rarely exceed this value. Compared with the operational version of the rain absorption calculation (Fig. 5), the absorption is found here to be weaker by around a factor of two, when averaged across the frequency band. Thus, for a given set of T_b observations, the current operational algorithm tends to assign too much of the brightness (and hence, absorption) to the rain contribution, and therefore too little to the wind (and hence, surface emissivity).

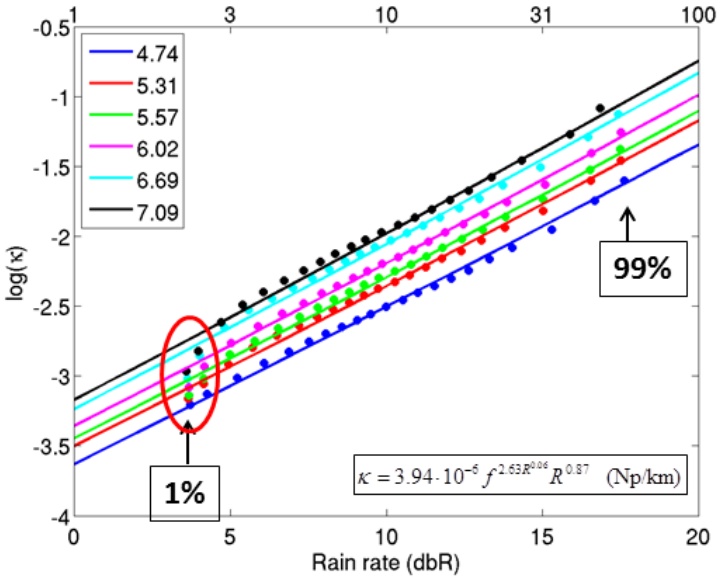

Figure 4. Linear fits between the absorption coefficient (κ) and rain rate (R) are provided in a logarithmic reference frame as a function of SFMR frequency. The lowest 1% and top 1% of the data are indicated to show the limits of the relationship. The associated κ-R equation is also included in the figure.

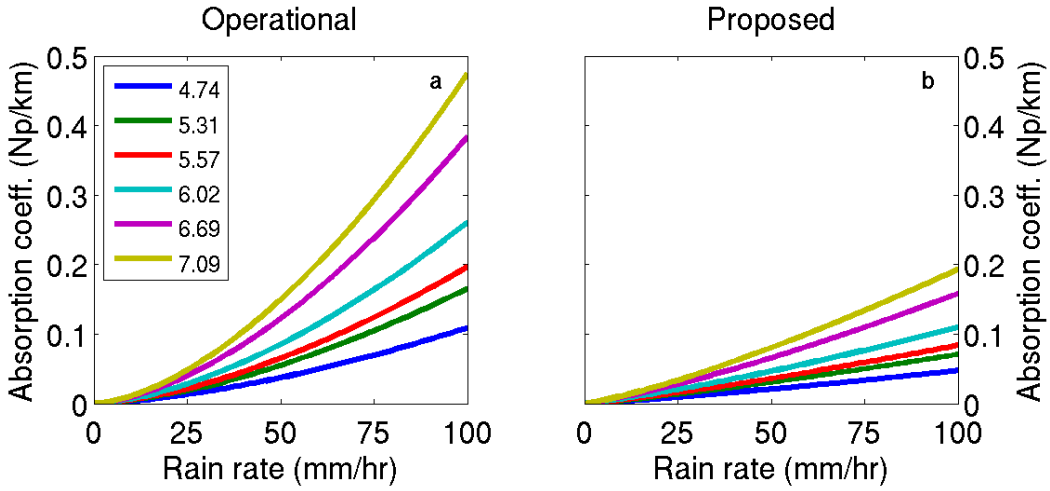

Figure 5. Operational (a) and proposed (b) absorption coefficient (κ, Np km^{-1} , ×10^{-4}) as a function of SFMR channel frequency is shown in relation to the rain rate. The spread in the proposed κ indicates there is less of the brightness temperature attributed to absorption as rain rate increases.

Task 3:

The proposed changes to the rain-absorption portion of the algorithm show more notable differences than those provided by the wind-emissivity update. These differences suggest that the rain signal being attributed to absorption is problematic in the current operational version. In order to quantify the improvements and changes of the new GMF using the updated wind-emissivity and rain-

absorption models, the new GMF was used to recalculate the SFMR wind speed and rain rate for the same pairs used in the operational database. One notable aspect was that the dynamic range of retrieved rain rates was limited due to the biased absorption model function, where maximum rain rates rarely exceeded 60 mm hr^{-1}, which is relatively low compared to other in situ observations of rain. The distribution of the current operational and the updated rain rates are provided in Figure 6. Overall, the updated version increases the variance of retrieved rain rates and increases the maximum attainable rain rate from 59 mm hr^{-1} to 91 mm hr^{-1}. As Jiang et al (2006) found, the operational SFMR rain rates tend to be biased low at high rain rates, and because we see this increase in the maximum, we would expect that this bias has been largely removed, especially since the updated rain rates compare better with other rain data.

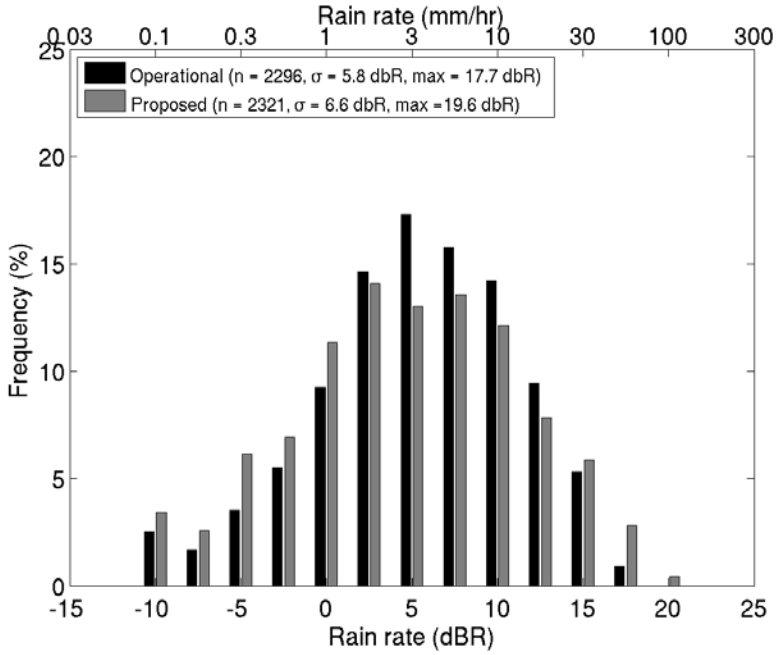

Figure 6. Histograms for the operational (black) and proposed (gray) rain rates are shown. These rain rates are displayed in dBR but the equivalent rain rate values in mm hr^{-1} are also provided for reference along the top axis. The range of achievable rain rates is expanded under the proposed update, where the maximum rain rate increases by nearly 2 dB or ~30 mm hr^{-1}.

For the examination of SFMR wind speed improvements, we compare several scenarios between the operational and updated algorithms. SFMR wind speeds, as with the rain rates, are recomputed using the revised algorithm, and the improvement in retrieval accuracy over the operationally-determined winds is evaluated based on a large sample (over 2700) of co-located GPS dropwindsonde surface wind measurements. Over all sampled wind speeds and rain rates, a significant improvement in

surface wind accuracy is found based on the correlation (slope of best-fit line increases from 0.88 to 0.98), while the root mean squared error decreases from 4.5 m s^{-1} to 3.9 m s^{-1}. The sample sizes are slightly different between the two versions since the numerical inversion procedure does not guarantee solutions for all measurements.

Further details about surface wind speed retrieval improvements are examined by stratifying according to wind speed greater than and less than the hurricane wind speed threshold (U_{sfc} = 33 m s^{-1}), and whether the measurement is inside or outside of precipitation. A rain/no-rain threshold of 2 mm hr^{-1} is chosen, since the SFMR is not particularly sensitive at these weak, stratiform rain rates. Significant reductions in SFMR overestimate are found for the weaker wind cases (U_{sfc} < 33 m/s), both outside of rain, where there is a decrease from +2.4 m s^{-1} to -0.2 m s^{-1}, and within rain, where there is a decrease from +2.8 m s^{-1} to +1.0 m s^{-1}, on average. Above the hurricane wind speed threshold, no significant changes in bias are found, and the mean biases for the both the operational and revised algorithms are not significantly different from zero.

In Figure 7, frequency distributions of SFMR wind speed bias are shown for measurements obtained in heavy precipitation (SFMR rain rate R > 20 mm hr^{-1}). As for all rain conditions for wind speeds greater than hurricane force, no statistically significant biases are found in either the operational or revised algorithm retrievals (Fig. 7b). A significant reduction in mean bias from +5.1 m s^{-1} to +3.7 m s^{-1} for wind speeds less than hurricane force is found by applying the revised algorithm, although a significant bias remains.

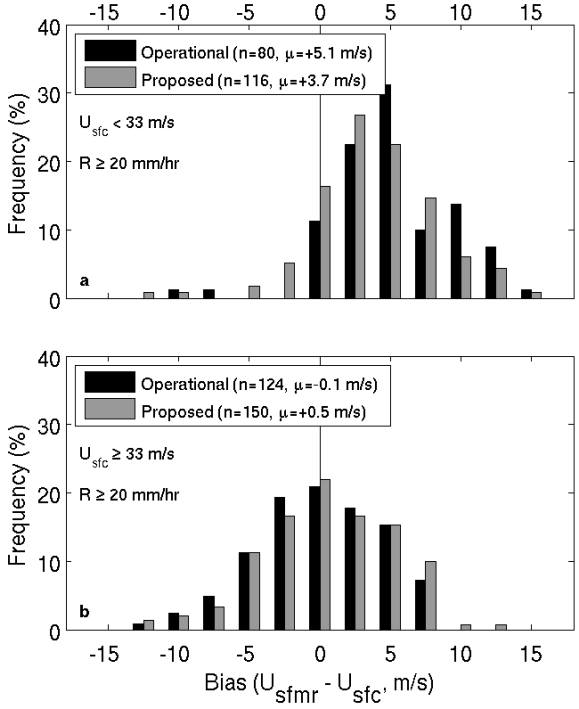

Figure 7. Histograms of the operational (black) and proposed (gray) wind speed bias for weaker (< 33 m s^{-1}) and stronger (≥ 33 m s^{-1}) winds for heavy precipitation conditions (≥ 20 mm hr^{-1}). Mean bias and population size are provided for each histogram.

Additionally, focus was placed on wind speed transition zones between tropical depression and tropical storm wind speeds (i.e. ± 4 m s^{-1} of 17 m s^{-1}) and between tropical storm and hurricane wind speeds (i.e. ± 4 m s^{-1} of 33 m s^{-1}). The wind speed bias as a function of rain rate for these two conditions for the operational and updated version is provided in Fig. 8. For the tropical storm transition, there is a consistent reduction in the bias at all rain rates, but the significance at rain rates >30 mm hr^{-1} may be reduced due to the number of pairs used in the bias calculation. Similarly to Fig. 7, there is still bias on the order of ~3-5 m s^{-1} within the heaviest precipitation. For the hurricane transition zone, there are minimal differences in the bias between the operational and proposed versions. This result is consistent with the results shown in Fig. 7 that indicates no significant change in wind speeds between the two versions regardless of the rain rate, despite the slight high bias at higher rain rates.

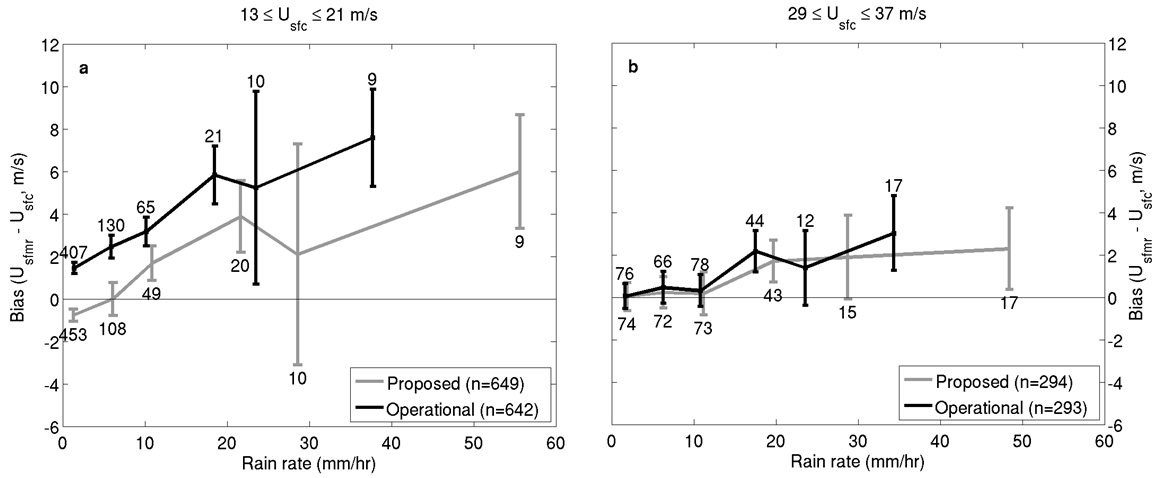

Figure 8. In (a), bin-averaged wind speed bias (U_{sfmr}-U_{sfc}, m s^{-1}) as a function of rain rate for the operational (black) and proposed (gray) SFMR wind speeds at the transition zone between tropical depression and tropical storm winds ($13 \leq U_{sfc} \leq 21$, m s^{-1}) is shown. In (b), the transition zone between tropical storm and hurricane winds ($29 \leq U_{sfc} \leq 37$, m s^{-1}) is provided in a similar manner to (a). The number of pairs and standard deviation (error bars) are provided for each bin.

Because there still remains some high bias in the heaviest precipitation at weak wind speeds, we developed a second bias correction model that uses the updated algorithm. The development utilizes the same procedures in prior reports documenting the bias model. Figure 9 shows the new bias correction model based on this new algorithm and Table 2 provides the respective coefficients for the equation in units of m s^{-1} and knots. This bias correction model is intended to apply to wind speeds less than hurricane strength and heavy rain rates as this is the region where the updated algorithm still produces a reduced but high bias that is not within the SFMR noise constraints.

	a_1	a_2	a_3	a_4
Units: m s^{-1}	-1.2957	6.66×10^{-2}	1.573×10^{-1}	-3.00×10^{-3}
Units: knots	-2.5188	6.66×10^{-2}	3.059×10^{-1}	-3.00×10^{-3}

Table 2. The coefficients of the new bias correction model that utilizes the updated SFMR algorithm wind speeds and rain rates. Coefficients are presented in units of m s^{-1} and knots. For the columns, a_1 is the final term in the equation similar to Eq. (1), a_2 is the first term in Eq. (1), a_3 is the second term in Eq. (1), and a_4 is the third term in Eq. (1).

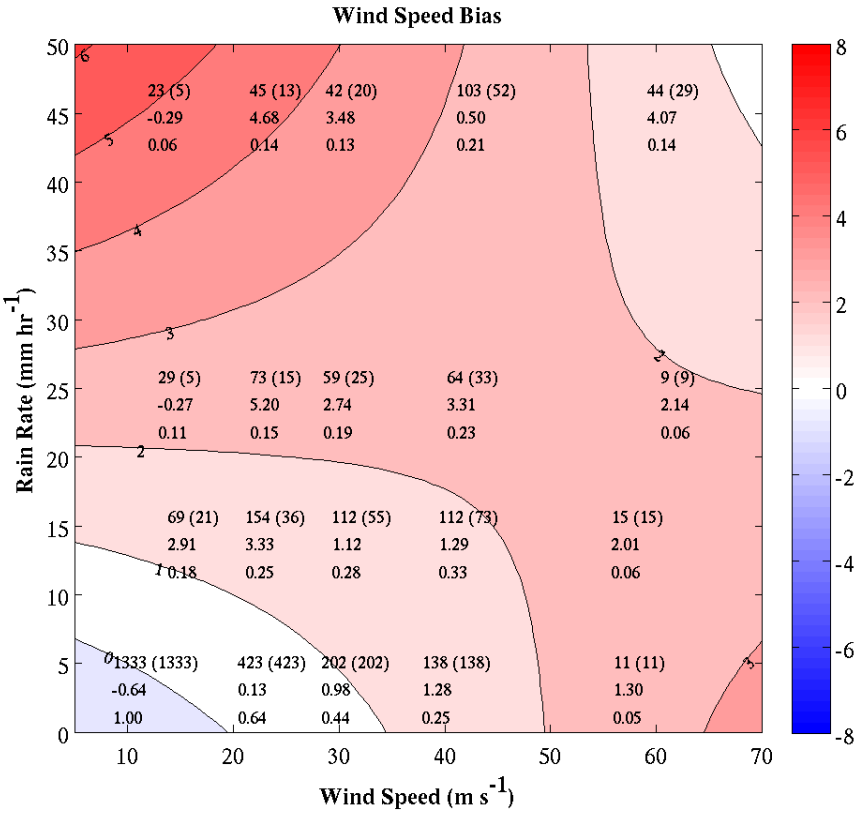

Figure 9. New bias correction model graphic presented in similar fashion to Fig. 1. The relevant corrections are those found at weak winds.

Task 4:

The objective of transferring the updated algorithm to the respective agencies is still on the table but has been postponed until Spring 2014. All information and results are available to NHC and the respective agencies, but will not be needed for operations until the 2014 Atlantic hurricane season. Currently, we have a manuscript documenting the proposed algorithm upgrade in peer review.

Summary of recommendations:

Based on the results of this project, we are recommending the following for consideration by the JHT committee:

1. Implement the revised algorithm for real-time SFMR retrievals during the 2014 hurricane season. This requires a modification to the SFMR processor software code. Coordination among all relevant groups (AFRC/53rd WRS, NOAA/AOC, Prosensing Inc.) shall be conducted, including providing code fragments where necessary.
2. Upon calculating the SFMR wind speed using the new algorithm, perform a final bias correction

as detailed in this report.

3. Include these final corrected SFMR wind and rain retrievals in the HDOB messages for real-time operations.
4. Periodically revisit the statistical bias correction as new data become available, ideally on an annual basis.

References:

Jiang, H., P. G. Black, E. J. Zipser, F. D. Marks, and E. W. Uhlhorn, 2006: Validation of Rain-Rate Estimation in Hurricanes from the Stepped Frequency Microwave Radiometer: Algorithm Correction and Error Analysis. *J. Atmos. Sci.*, **63**, 252–267.

Jorgensen, D. P., and P. L. Willis, 1982: A *Z-R* relationship for hurricanes. *J. Appl. Meteor.*, **21**, 356 – 366.

Monahan, E. C., 1971: Oceanic Whitecaps. *J. Phys. Oceanogr.*, **1**, 139-144.

Rinehart, R. E., 2004: Radar for Meteorologists, Fourth Edition. Rinehart Publications, 482 pp.

Rosenfeld, D., D. B. Wolff, and D. Atlas, 1993: General Probability-matched Relations between Radar Reflectivity and Rain Rate. *J. Appl. Meteor.*, **32**, 50-72.

———, ———, and E. Amitai, 1994: The Window Probability Matching Method for Rainfall Measurements with Radar. *J. Appl. Meteor.*, **33**, 682-693.

Ross, D. B. and V. Cardone, 1974: Observations of Oceanic Whitecaps and their Relation to Remote Measurements of Surface Wind Speed. *J. Geophys. Res.*, **79**, 444-452.

Uhlhorn, E. W., and P. G. Black, 2003: Verification of Remotely Sensed Sea Surface Winds in Hurricanes. *J. Atmos. Oceanic Technol.*, **20**, 99–116.

Uhlhorn, E. W., P. G. Black, J. L. Franklin, M. Goodberlet, J. Carswell, and A. S. Goldstein, 2007: Hurricane Surface Wind Measurements from an Operational Stepped Frequency Microwave Radiometer. *Mon. Wea. Rev.*, **135**, 3070–3085.

Webster Jr., W. J., T. T. Wilheit, D. B. Ross, and P. Gloersen, 1976: Spectral Characteristics of the Microwave Emission from a Wind-driven Foam-covered Sea. *J. Geophys. Res.*, **81**, 3095-3099.

Zhang, J. A. and E. W. Uhlhorn, 2012: Hurricane Sea Surface Inflow Angle and Observation-Based Parametric Model. *Mon. Wea. Rev.*, **140**, 3587-3605.